Numerical investigation of turbulent combustion with hybrid enrichment by hydrogen and oxygen

Zouhaier Riahi, Ibtissem Hraiech, Jean-Charles Sautet, Sassi Ben Nasrallah

Version of Record: https://www.sciencedirect.com/science/article/pii/S0360319919343745
Manuscript_a87c984472a2a0cf14dd0500565f207c

Numerical investigation of turbulent combustion with hybrid enrichment by hydrogen and oxygen

Zouhaier Riahi [a,c]***, Ibtissem Hraiech*** [b,c]***, Jean-Charles Sautet*** [c]***, Sassi Ben Nasrallah*** [b]

[a] *Research and Technology Center of Energy, Laboratory of Wind Energy Master and Waste Energy Recovery (LMEEVED), Hammam-Lif 2050, Tunisia*

[b] *National Engineering School of Monastir, LESTE, Monastir, Tunisia*

[c] *Aerothermochemistry Interprofessional Research Complex (CORIA), University of Rouen , France*

Corresponding author: Zouhaier.Riahi@crten.rnrt.tn

Abstract

In this study, the NG+H_2/air+O_2 turbulent flame is numerically investigated using the Computational Fluid Dynamics CFD code. The modulation of combustion and radiation is performed respectively by the Eddy Dissipation Model and the Discrete Ordinate Model. The turbulence modeling is carried out by Shear Stress Transport (SST/k-ω) turbulence model. The H_2 amount in the fuel mixture varies under constant volumetric fuel flow between 0 and 60% and the oxidant is composed by 80% air and 20% pure oxygen. The results obtained show the hydrogen addition to Natural Gas improves the mixing between the reactants, reduces their residence time and reduces the length and thickness of the flame. On the other hand, the hydrogen enrichment minimizes the CO_2 and CO production and increases the NO_x level.

Keywords: NG+H_2/air+O_2 turbulent flame; Eddy Dissipation Model; Discrete Ordinate Model; (SST) k-ω turbulence model; hydrogen enrichment

1. Introduction

Natural Gas is commonly used for heat production, electricity production and in automobile and rocket engines. The main objective of researchers is to improve the combustion efficiency and to ensure a clean combustion process in industries. The hydrocarbon enrichment by hydrogen, the oxidant enrichment by oxygen, the MILD combustion... are very advanced combustion technologies can used to achieve these objectives. The hydrogen is an energy vector of the future, it can be partially substituted for hydrocarbons, because of its high flammability, high combustion velocity, low ignition energy, low density and high molecular diffusivity [1, 2]. The hydrogen is non-polluting and does not emit carbon dioxide, carbon

monoxide and sulfur oxide. In recent years, the hydrocarbon / hydrogen mixture became the subject of extensive research. Many experimental and numerical studies has been done to present a better understand its combustion characteristics. The hydrogen addition to hydrocarbon showed an increase in the flame temperature, a reduction in the length and the thickness of the flame and improves the auto-ignition characteristics [3, 4]. The increase of hydrogen in the fuel mixture reduces the CO and CO_2 emissions, but promotes the NO_x production [5, 6]. Experimental studies were performed on a spark ignition engine operates on natural gas [7-9]. These studies show that the concentrations of CO and CO_2 emissions could be reduced with the addition of hydrogen to natural gas. However, the increase of the flame propagation velocity and the increase in the combustion temperature promote the formation of NO_x. The hydrogen addition to methane in Moderate or Intense Low-oxygen Dilution (MILD) condition [10-12] leads to improve mixing, increase in the flame entrainment, increase in reaction intensities, increase in the mixture ignitability and increase in the rate of heat release. The effects of hydrogen addition on stability of lean natural gas–air flame were studied and the results showed that the lean stability limit were extended by hydrogen addition [13-15] due to the increase of OH concentration in the flame. The natural gas-hydrogen composite fuel in a turbulent diffusion flame is studied experimentally [16] in terms of flame stability, flame length, flame structure and exhausts species concentrations.

The oxygen enrichment reduces the nitrogen amount in the reaction, which increases the flame temperature, reduce the time of increasing temperature in furnace and decrease the volume of exhaust gas. The energy necessary for heating the nitrogen decreases with oxygen enrichment. Many authors [17, 18] observed a decrease of 26% in fuel consumption when the oxygen content changing from 21 to 30% by volume, for a furnace temperature 1200°C.

The oxygen addition to the oxidant minimizes the losses of unburned gas (CO and C_xH_y) and increase the combustion efficiency. The propagation velocity of a laminar flame front increase from 0.3 m/s of methane/air flame to 0.9 m/s of methane/air + 30% O_2 flame and reach 3.9 m/s of methane/100%O_2 flame [19-21]. The Oxygen enrichment increases significantly the flame stability [22-27] and showed that the flame length decreases when the oxygen content in the oxidant increases. The effects of hybrid hydrogen and oxygen enrichment on the flame structure, on the flow dynamics along the flame and on the pollutant emissions at stoichiometry and lean conditions are studied experimentally [28, 29]. They showed that the mixed enrichment of hydrogen and oxygen favors the stability and existence flame in important velocity oxidant injection and in very poor regime.

In the present paper, NG+H_2/air+O_2 turbulent flame is numerically investigated. The main objective of this work consists on highlighting the effect of hybrid hydrogen and oxygen enrichment on the mixing and on CO_2, CO and NO_x production of the NG + H_2 / air + O_2 flame. In the first part, the numerical code is validated using the experimental configuration of Riahi et al. [28, 29]. The second parts of this works, shows numerically the effect of hydrogen enrichment on NG+H_2/air+O_2 flame characteristics.

Nomenclatue

d_{ox}	diameter of oxidant jet, mm	*Greek symbols*	
d_{Fuel}	diameter of fuel jet, mm	ρ	density, kg m^{-3}
T	temperature, K	μ	dynamic molecular viscosity, kg s^{-1} m^{-1}
p	static pressure, Pa	ν	kinematic viscosity, m^2 s^{-1}
u_i	mean velocity components along x_i	k	turbulent kinetic energy, m^2s^{-2}
	directions, ms^{-1}	υ	stoichiometric coefficient
u'_i	fluctuating velocity components, m s^{-1}	δ_{ij}	Kronecker symbol
D	molecular diffusion coefficient, m^2s^{-1}	τ_{ij}	stress tensor, kgs^{-2} m^{-1}
Y_m	mole fraction of species "m"		
R_m	net production rate of species "m"		
E	total mass energy, J/kg	*Other symbols*	
g	gravity acceleration, ms^{-2}	~ Favre average	
h	specific enthalpy, J kg^{-1}	— Reynolds	
Sc	turbulent Schmidt number	average	
M_m	molecular weight of species "m"		
r	radial position, m		
r_0	fuel jet radius, m		

2. Presentation of the computational domain

The experimental configuration studied by Riahi et al. [28, 29] is used to study a confined turbulent reactive flow issuing from coaxial burner figure.1. The Natural gas and hydrogen mixture is injected through an internal cylindrical nozzle of diameter d_{Fuel} equal to 6 mm. The air and oxygen mixture is injected through an annular nozzle with a diameter d_{ox} equal to 18 mm. The burner is located on the bottom wall of the combustion chamber, which is a 1200 mm high vertical tunnel with square cross section (600* 600 mm^2). In this work, the numerical study is interested by the turbulent diffusion flame (NG + H_2 / air + O_2). In the fuel jet, the volume ratio of hydrogen varies between 20% and 60%. In the oxidant jet, the oxygen volume fraction is 0.36 and the nitrogen volume fraction is 0.64. The compositions by volume of Natural Gas are indicated in table.1.

3. Numerical formulation

In this study, turbulent, incompressible and multi-species reactive flow is numerically studied in 2D axi-symmetric geometry. The stationary state of conservation equations of mass, momentum, species and energy are solved numerically. The density variation in the flow is taken account using the Favre decomposition.

3.1. Conservative governing equations

Following the above assumptions, the mass and momentum conservation equations are written as follows:

$$\frac{\partial\left(\overline{\rho}\tilde{u}_{\mathrm{j}}\right)}{\partial x_j}=0 \tag{1}$$

$$\frac{\partial\left(\overline{\rho}\tilde{u}_{\mathrm{i}}\tilde{u}_{\mathrm{j}}\right)}{\partial x_{\mathrm{j}}}=-\frac{\partial\overline{p}}{\partial x_{\mathrm{i}}}+\frac{\partial\tilde{\tau}_{\mathrm{ij}}}{\partial x_{\mathrm{j}}}-\frac{\partial\left(\overline{\rho u_{\mathrm{i}}^{''}u_{\mathrm{j}}^{''}}\right)}{\partial x_{\mathrm{j}}}+\overline{\rho}g_{\mathrm{i}} \tag{2}$$

$$\tilde{\tau}_{\mathrm{ij}}=\overline{\mu}\left(\frac{\partial\tilde{u}_i}{\partial x_{\mathrm{j}}}+\frac{\partial\tilde{u}_{\mathrm{j}}}{\partial x_i}\right)-\frac{2}{3}\overline{\mu}\left(\frac{\partial\tilde{u}_i}{\partial x_{\mathrm{j}}}\right)\delta_{ij} \tag{3}$$

The Reynolds stresses - are given by [24]:

$$-\overline{\rho u_i^{''}u_j^{''}}=\mu_{\mathrm{t}}\left(\frac{\partial\tilde{u}_{\mathrm{i}}}{\partial x_{\mathrm{j}}}+\frac{\partial\tilde{u}_{\mathrm{j}}}{\partial x_i}\right)-\frac{2}{3}\left(\overline{\rho}k+\mu_{\mathrm{t}}\frac{\partial\tilde{u}_i}{\partial x_i}\right)\delta_{ij} \tag{4}$$

with μ_{t} is the turbulence viscosity and k is the turbulent kinetic energy.

3.2. Turbulence modeling

The SST k-ω turbulent model presented by Wilcox [30] and Menter [31] is used to model the turbulent kinetic energy k and the specific dissipation rate ω. For the SST k-ω turbulent model, the turbulent viscosity is modified to account for the transport of the principal turbulent shear stress. This characteristic gives the SST k-ω model an advantage in terms of performance over both the standard k-ω model and the standard k-ε model. On the other hand, the addition of a cross-diffusion term in the ω equation ensures the model equations behave appropriately in both the near-wall and far-field zones. Huang et al. [32] have studied the influences of the turbulence model on the transverse slot injection flow field. They showed that, the numerical results obtained by the SST k-ω turbulence model match better with the

experimental data than the other turbulence models used. The transport equations for k and ω expressed by:

$$\frac{\partial}{\partial x_i}\left(\rho\tilde{u}_i k\right)=\frac{\partial}{\partial x_j}\left(\Gamma_k\frac{\partial k}{\partial x_j}\right)+G_k-L_k+S_k \tag{5}$$

$$\frac{\partial}{\partial x_i}\left(\rho\tilde{u}_i \omega\right)=\frac{\partial}{\partial x_j}\left(\Gamma_\omega\frac{\partial \omega}{\partial x_j}\right)+G_\omega-L_\omega+D_\omega+S_\omega \tag{6}$$

The effective diffusivities for the SST k-ω model are given by

$$\Gamma_k=\mu+\frac{\mu_t}{\sigma_k} \tag{7}$$

$$\Gamma_\omega=\mu+\frac{\mu_t}{\sigma_\omega} \tag{8}$$

where σ_k and σ_ω are the turbulent Prandtl number for k and ω respectively and μ_t the turbulent viscosity

$$\sigma_k=\frac{1}{\frac{F_1}{\sigma_{k,1}}+\frac{\left(1-F_1\right)}{\sigma_{k,2}}} \tag{9}$$

$$\sigma_\omega=\frac{1}{\frac{F_1}{\sigma_{\omega,1}}+\frac{\left(1-F_1\right)}{\sigma_{\omega,2}}} \tag{10}$$

$$\mu_t=\frac{\rho k}{\omega}\frac{1}{\max\left[\frac{1}{\alpha^*},\frac{SF_2}{\alpha_1\omega}\right]} \tag{11}$$

S is the strain rate magnitude, α* and the blending functions F1, F2 are given by

$$\alpha^*=\alpha_\infty^*\left(\frac{\alpha_0^*+\frac{R_{et}}{R_k}}{1+\frac{R_{et}}{R_k}}\right) \tag{12}$$

$$F_1 = \tanh\left(\Phi_1^4\right) \tag{13}$$

$$F_1 = \tanh\left(\Phi_2^2\right) \tag{14}$$

Where

$$R_{et} = \frac{\rho k}{\mu \omega} \tag{15}$$

$$\Phi_1 = \min\left[\max\left(\frac{\sqrt{k}}{0.09\omega y}, \frac{500\mu}{\rho y^2 \omega}\right), \frac{4\rho k}{\sigma_{\omega,2} D_\omega^+ y^2}\right] \tag{16}$$

$$\Phi_2 = \max\left[2\frac{\sqrt{k}}{0.09\omega y}, \frac{500\mu}{\rho y^2 \omega}\right] \tag{17}$$

y is the distance to the next surface and D^+_ω is the positive portion of the cross-diffusion term.

$$D_\omega^+ = \max\left[2\rho\frac{1}{\sigma_{\omega,2}}\frac{1}{\omega}\frac{\partial k}{\partial x_j}\frac{\partial \omega}{\partial x_j}, 10^{-20}\right] \tag{18}$$

The term G_k represents the production of turbulence kinetic energy

$$G_k = -\rho \overline{u_i' u_j'} \frac{\partial u_j}{\partial x_i} \tag{19}$$

The term G_ω represents the production of ω and is given by

$$G_\omega = \frac{\alpha}{\nu_t} G_k \tag{20}$$

where

$$\alpha = \frac{\alpha_\infty}{\alpha^*}\left(\frac{\alpha_0 + \frac{R_{et}}{R_\omega}}{1 + \frac{R_{et}}{R_\omega}}\right) \tag{21}$$

The term L_k and L_ω represents the dissipation of turbulence kinetic energy and dissipation of ω respectively

$$L_k = \rho\beta^* k\omega \tag{22}$$

$$L_\omega = \rho\beta\omega^2 \tag{23}$$

Where $$\beta^* = \beta_i^*\left[1+\xi^* F(M_t)\right] \tag{24}$$

$$\beta = \beta_i\left[1-\frac{\beta_i^*}{\beta_i}\xi^* F(M_t)\right] \tag{25}$$

$$\beta_i^* = \beta_\infty^*\left(\frac{\frac{4}{15}+\left(\frac{R_{et}}{R_\beta}\right)^4}{1+\left(\frac{R_{et}}{R_\beta}\right)^4}\right) \tag{26}$$

$$\beta_i = F_1\beta_{i,1} + (1-F_1)\beta_{i,2} \tag{27}$$

$$F(M_t) = \begin{cases} 0 & M_t \le M_{t0} \\ M_t^2 - M_{t0}^2 & M_t > M_{t0} \end{cases} \tag{28}$$

The term D_ω represents the Cross-Diffusion Modification is given by

$$D_\omega = 2\left(1-F_1\right)\rho\sigma_{\omega,2}\frac{1}{\omega}\frac{\partial k}{\partial x_j}\frac{\partial \omega}{\partial x_j} \tag{29}$$

Model Constants

$\sigma_{k,1} = 1.176$; $\sigma_{k,2} = 1$; $\sigma_{\omega,1} = 2$; $\sigma_{\omega,2} = 1.168$; $\alpha_1 = 0.31$; $\alpha^*_\infty = 1$; $\alpha^*_0 = 0.024$; $\alpha_0 = 1/9$; $\alpha_\infty = 0.52$; $R_w = 2.95$; $\beta_{i,1} = 0.075$; $\beta_{i,2} = 0.0828$; $\beta_i = 0.072$; $\beta^*_\infty = 0.09$; $R_\beta = 8$; $R_k = 6$; $\zeta^* = 1.5$; $M_{t0} = 0.25$

3.3. Combustion modeling

To simulate the studied reacting flow, the Eddy Dissipation Model (EDM) is considered. The species and energy conservation equations are written in the following form [33]:

$$\frac{\partial}{\partial x_j}\left(\overline{\rho}\overline{u}_i\overline{Y}_m\right)=\frac{\partial}{\partial x_j}\left(\left(\overline{\rho}D+\frac{\mu_t}{S_{ct}}\right)\frac{\partial\overline{Y}_m}{\partial x_j}\right)+R_m \tag{30}$$

$$\frac{\partial}{\partial x_i}\left(\overline{u}_i\left(\overline{\rho}\overline{E}+\overline{p}\right)\right)=\frac{\partial}{\partial x_i}\left(\left(\lambda+\frac{c_p\mu_t}{Pr_t}\right)\frac{\partial\overline{T}}{\partial x_i}-\sum_m h_m J_m+\overline{u}_i\,\tilde{\tau}_{ijeff}\right)+S_h \tag{31}$$

$$\tilde{\tau}_{ij_{eff}}=\overline{\mu_{eff}}\left(\frac{\partial\tilde{u}_i}{\partial x_j}+\frac{\partial\tilde{u}_j}{\partial x_i}\right)-\frac{2}{3}\overline{\mu_{eff}}\left(\frac{\partial\tilde{u}_i}{\partial x_j}\right)\delta_{ij} \tag{32}$$

S_{ct} the turbulent Schmidt number ($S_{ct}=\mu/\sigma D$) and R_m the reaction rate of species m.

h the enthalpy of species m, J_m is the diffusion flux of species m and S_h is the source term due to radiation heat transfer to wall boundaries and exchange with the second phase and μ_{eff} represent the effective viscosity ($\mu_{eff}=\mu+\mu_t$).

The interaction model between turbulence and reaction chemistry (EDM) based on the work of Magnussen and Hjertager [34], Where the net production rate of species "m" by the reaction "r" ($R_{m,r}$) is given by the smaller of the following two expressions:

$$R_{m,r}=\upsilon'_m M_m A\rho\frac{\varepsilon}{k}\min_R\left(\frac{Y_R}{\upsilon'_R M_R}\right) \tag{33}$$

$$R_{m,r}=\upsilon'_m M_m AB\rho\frac{\varepsilon}{k}\frac{\sum_P Y_P}{\sum_j^N \upsilon''_j M_j} \tag{34}$$

where A and B are empirical constant, υ' et υ" are the stoichiometric coefficients for reactant and product in reaction, Mm is the molecular weight of species m, Yp and YR are the mass fraction of the product species P and the particle reactant R. The chemistry is assumed to be infinitely fast compared to the mixing of the reactants. To model the combustion of gas, we employed three-step mechanism. The chemical equations for the combustion are defined by:

$$C_xH_y + 0.5\,(x + 0.5\,y)\,O_2 \rightarrow x\,CO + 0.5\,y\,H_2O \tag{35}$$

$$H_2 + 0.5\,O_2 \leftrightarrow H_2O \tag{36}$$

$$CO + 0.5\,O_2 \leftrightarrow CO_2 \tag{37}$$

3.4. Radiation modeling

The discrete ordinate "DO" radiation model is suitable for optically thin problems (aL < 1) [33]. Where, ' L ' corresponds to the combustor diameter and 'a' the absorption coefficient. In the current study, L equal to 0.3 m and a < 1. The discrete ordinate "DO" radiation model [35-37] and absorption coefficient of weighted sum of gray gas "WSGGM" model [38, 39] is used in this work.

3.5. NO_x modeling

In the present study, the mass transport equation for NO species is solved, taking into account convection, diffusion, production and consumption of NO

$$\frac{\partial}{\partial x_j}\left(\overline{\rho}\tilde{u}_i \tilde{Y}_{NO}\right) = \frac{\partial}{\partial x_j}\left(\overline{\rho} D \frac{\partial \tilde{Y}_{NO}}{\partial x_j}\right) + \tilde{S}_{NO} \tag{38}$$

4. Numerical method and Boundary conditions

The mathematical modeling is based on a set of coupled conservation equations of mass, momentum, energy, and chemical species transport and reactions. In this work, the turbulence modeled using the SST *k*-ω turbulent model. The simulation of gas phase combustion is based on the multi-step chemical reactions where Eddy-Dissipation Model is used to calculate the interaction between turbulence and chemical reactive flows and the radiation heat transfer is modeled by the Discrete Ordinate radiation model. The finite volume method with a second order upwind scheme is used to discrete the conservative governing equations. The algorithm SIMPLE was adopted for the coupling between velocity and pressure. The convergence criterion of residuals was taken equal to 10^{-6} for energy and 10^{-3} for all other equations.

In the current study, total 9 species, such as CH_4, C_2H_6, C_3H_8, O_2, CO, CO_2, H_2, H_2O and N_2 are used in this model. A total number of 25650 quadrilateral cells were generated using non-uniform grid. The considered mesh was sufficiently dense in the reaction zone and less tight away from this zone.The computational domain is limited by the symmetry axis, the gas and oxidant inlet, the walls and the exhaust gas (pressure outlet) figure.2. The boundary conditions illustrated in figure.2 are summarized in table.2

The mesh quality affects directly the accuracy of the simulation results. In this study, several meshes were tested (15500 cells, 25650, 35300 cells, and 50250 cells), to ensure numerical results independency from grid density. Figure.3 illustrates the temperature profiles for different tested meshes. In this figure, the mesh having 15500 cells provides a temperature profile far from the rest of the other meshes. While, when the mesh is refined, the numerical

temperature profiles become closer. From a number of 25500 cells, the temperature profiles become independent the mesh. As a consequence, this mesh is chosen.

5. Results and discussions

In this study, the effect of hydrogen and oxygen enrichment on Non-premixed flame issued by coaxial burner is investigated numerically. The experimental results found by Riahi et al [28, 29] are used to validate the numerical results. The coaxial burner configuration was selected, because this burner type is widely used in industries. The numerical results are validated in terms of temperature and velocity.

5.1. Numerical validation

Riahi et al [28] were used a K-type thermocouple to measure the exhaust temperature. This thermocouple is placed at the furnace outlet to measure the fumes average temperature. In this numerical work, the exhaust temperature evolution is validated by these experimental results (figure.4). This validation gives a good agreement between the experimental and numerical results.

The longitudinal velocity profile is compared by the experimental results of Riahi et al [28, 29]. Figure.5 illustrates the experimental and numerical radial evolution of longitudinal velocity along the flame. Noticing that, for each height (y = 20 mm, 50 and 100 mm), there is a good agreement between the experimental and numerical profiles. Along the flow, the longitudinal velocity profile having a parabolic shape, decreasing radially and vanishes away to the burner injectors.

5.2. Hydrogen enrichment effect on the flame temperature

The temperature distribution in the studied geometry is a good indicator of the flame behavior. Figure.6 illustrates the temperature field in the flame from a coaxial burner as a function of hydrogen content in natural gas. This figure shows that the flame temperature depends on the hydrogen amount in the fuel mixture (NG + H_2). Grace to its low density and high diffusivity, the hydrogen addition becomes a very important factor promotes the interaction between the fuel and oxidant jets and improves the mixing between them. Consequently, the hydrogen adding to the fuel mixture increases the flame temperature and reducing its length. The temperature variation curves along the burner axis (figure.7) allows to determine the positions of the high temperatures in the flame as shown in table.3

The peaks temperature positions indicate a clear idea on the flame length. The pure natural gas flame is longer and less hot compared to the flame of natural gas enriched by hydrogen. Indeed, at 100% natural gas the flame temperature is 2429 ° K with a length of 436 mm, On the other hand with an enrichment of 60% by hydrogen, the temperature increases to 2644 ° K and the length decreases to 310 mm. These variations of the flame length and temperature are related to the properties of hydrogen. The hydrogen combustion reaction is faster, which leads to rapid consumption of the reagents, consequently a decrease in the flame length. So, the hydrogen reaction releases a significant heat amount which leads to an increase in the flame temperature.

The term stoichiometric line it's the all positions of the high temperatures along the flame.

These lines are shown in figure.8 depending on the hydrogen percentage in the fuel mixture. They are shifted down when the hydrogen content in the fuel increases. These lines are important indicators to estimate the end of the complete mixing zone between fuel and oxidant, and consequently give an estimate of the flame length.

5.3. Species evolution in the reaction

In this paragraph, the fuel is a natural gas and hydrogen mixture. The radial profiles of the fuel and oxygen mole fractions along the flame (y = 0.01 m, y = 0.2 m, y = 0.31 m and y = 0.436 m), as a function of hydrogen content in the fuel, are shown in figure.9. For the studied configurations, the shape of each mole fraction profile of the fuel (NG + H_2) starts with a maximum which represents the maximum fuel quantity not consumed by the reaction. This maximum located on the burner axis. These maximums decrease along the flame and vanish at the end of reaction. Thus, these maximums strongly related to the amount of hydrogen added to the fuel. The increase in hydrogen content in the fuel causes a reduction in the maximum molar fraction of the fuel, and the reactants consumption becomes faster. Therefore, the hydrogen addition to the fuel promotes the reaction rate. The molar fraction fuel profiles are gradually decreasing up to the intersection point with the molar fraction oxygen profiles. This point represents the internal mixing point between fuel and oxidant. In the combustion reaction, the internal mixing point shifts towards the fuel jet, when the fuel contains more hydrogen. The hydrogen addition is an important factor promotes the diffusion between fuel and oxidant. So, with the hydrogen addition, we can have a short and thin flame. Both profiles of fuel and oxygen mole fraction give an interesting idea about the mixing quality between the reactants. In fact, at the mixing point, the mixture between the reactants almost to the stoichiometric and the flame front located at this point. The zone located at the

left of the mixing point, where the fuel is dominant, represents the rich combustion zone and the zone located at the right of the mixing point, where the oxygen is dominant, represents the lean combustion zone.

The radial profiles of CO_2 and CO mole fractions with different hydrogen amounts in the fuel mixture are illustrated in figure.10. The molar fractions of CO_2 and CO strongly depend on the mixing quality between fuel and oxidant and depend on the hydrogen content in the fuel. At an intermediate height in the flame (y = 0.2m) and at the fuel jet axis ($r / r_0 = 0$), the CO_2 mole fraction is minimal, by against, the CO mole fraction is maximal. On the fuel jet axis, the mixture between the reactants is rich which favors the CO production in this zone. In the internal mixing zone between the reactants, the CO_2 mole fraction reaches its maximum and the CO mole fraction begins to decrease. The maximum of CO_2 profile decreases with increasing hydrogen content in the fuel. Thus, the radial position of this maximum becomes closer to the fuel jet due to the high hydrogen diffusivity. Without hydrogen, the maximum mole fractions of CO_2 and CO are 0.0983 and 0.026. By cons, with a 60% of hydrogen content in the fuel, these maximums become respectively 0.066 and 0.017, leading to a decrease by 32.8% in the CO_2 production and 34.6% in CO production. The hydrogen enrichment promotes the mixture between the fuel and oxidant jets and optimizes the CO_2 and CO production. The decrease of CO_2 and CO maximums is due to the replacement of carbon atoms by hydrogen atoms.

The Nitrogen Oxides (NO_x) are formed mainly by chemical combination between oxygen and nitrogen, during a very high temperature combustion. Figure.11 shows the radial evolution of NO_x emissions as a function of hydrogen volume fraction in the fuel. This figure shows that, the hydrogen addition to natural gas encourages the increase of NO_x mole fraction in the internal mixing zone between fuel and oxidant. Where the temperature in this zone is very high. For pure Natural Gas combustion, the maximum mole fraction of NO_x is 0.710^{-3}, and for combustion of a mixture contains 60% of hydrogen is 1.3510^{-3}. Tabet et al [6] have been shown the same thing, that the hydrogen addition to the fuel promotes the production of NO_x in the flame.

6. Conclusion

This article is interested by the numerical study of the (Natural Gas + Hydrogen / Air + Oxygen) turbulent diffusion flame from a coaxial burner, and to have the influence of the hydrogen amount variation in the fuel on the flame structure, on the temperature distribution and on the emissions of atmospheric pollutants. The numerical approach employed in the

current study has been validated against the experimental data in the literature. We have come to the following conclusions:

- With a mixed oxidant, contains 80% air and 20% oxygen, the increase of the hydrogen content in the fuel reduces the flame length. such that, the addition of 60% hydrogen leads a reduction in the flame length by 29%
- The radial position of the maximum temperature becomes near the burner axis when the hydrogen addition increases. which shows that the hydrogen addition improves the mixing quality between the reactants
- The hydrogen addition promotes the flame temperature
- The hydrogen addition minimizes the formation of CO_2 and CO
- The presence of nitrogen in the reaction at high temperature promotes the NO_x formation

References

[1] A.R Choudhuri, S.R. Gollahalli, Combustion characteristics of hydrogen-hydrocarbon hybrid fuels, *International Journal of Hydrogen Energy 25 (2000) 451-462*

[2] F. Cozzi, A. Coghe, Behavior of hydrogen-enriched non-premixed swirled natural gas flames, *International Journal of Hydrogen Energy 31 (2006) 669-677*

[3] Y. Lafay, B. Renou, G. Cabot, M. Boukhalfa, Experimental and numerical investigation of the effect of H2 enrichment on laminar methane–air flame thickness, *Combustion and Flame 153 (2008) 540–61*

[4] C. Safta, C. Madnia, Autoignition and structure of non-premixed CH_4/H_2 flames: detailed and reduced kinetic models, *Combustion and Flame 144 (2006) 64–73*

[5] N. Kahraman, B. Ceper, SO. Akansu, K. Aydin, Investigation of combustion characteristics and emissions in a spark-ignition engine fuelled with natural gase hydrogen blends, *International Journal of Hydrogen Energy 34 (2009) 1026-1034*

[6] F. Tabet, B. Sarh, I. Gokalp, Hydrogen–hydrocarbon turbulent non-premixed flame structure, *International Journal of Hydrogen Energy 34 (2009) 5040–5047*

[7] BP. Van, JO. Keller, A hydrogen fuelled internal combustion engine designed for single speed/power operation, *International Journal of Hydrogen Energy 23 (1998) 603–609*

[8] S.O. Bade Shrestha, G.A. Karim, Hydrogen as an additive to methane for spark ignition engine applications, *International Journal of Hydrogen Energy 24 (1999) 577-586*

[9] M. Bysveen, Engine characteristics of emissions and performance using mixtures of natural gas and hydrogen, *Energy 32 (2007) 482-489*

[10] M. Mardani, S. Tabejamaat, Effect of hydrogen on hydrogen methane turbulent non-premixed flame under MILD condition, *International Journal of Hydrogen Energy* 35 (2010) 11324-11331

[11] A. Yashar, S. Tabejamaat, Effect of hydrogen on H_2/CH_4 flame structure of MILD combustion using the LES method, *International Journal of Hydrogen Energy 38 (2013) 3447-3458*

[12] M. Ayoub, C. Rottier, S. Carpentier, C. Villermaux, A.M. Boukhalfa, D. Honore´, An experimental study of mild flameless combustion of methane/hydrogen mixtures, *International Journal of Hydrogen Energy 37 (2012) 6912-6921*

[13] R.W. Schefer, Hydrogen enrichment for improved lean flame stability, *International Journal of Hydrogen Energy 28 (2003) 1131–1141*

[14] Cozzi F, Coghe A. Behavior of hydrogen-enriched non-premixed swirled natural gas flames. *International Journal of Hydrogen Energy 31 (*2006) 669–677

[15] A. Katoh, H. Oyama, K. Kitagawa, A.K. GUPTA, Visualization of OH radical distribution in a methane–hydrogen mixture flame by isotope shift/planar laser induced fluorescence spectroscopy, *Combustion Science and Technology 178 (2006) 2061–2074*

[16] S.A.A. El-Ghafour, A.H.E. El-dein, A.A.R. Aref, Combustion characteristics of natural gas-hydrogen hybrid fuel turbulent diffusion flame, *International Journal of Hydrogen Energy 35 (2010) 2556-2565*

[17] K.K. Wu, Y.C. Chang , C.H. Chen , Y.D. Chen, High-efficiency combustion of natural gas with 21–30% oxygen-enriched air, *Fuel 89 (2010) 2455-2462*

[18] G. Bisio, A. Bosio, G. Rubatto, Thermodynamics applied to oxygen enrichment of combustion air, *Energy Conversion and Management 43 (2002) 2589–2600*

[19] E. Charles, Jr. Baukal, Oxygen-Enhanced Combustion, Second Edition: CRC Press; 2013

[20] P. Dirrenberger, H. Le Gall, R. Bounaceur, O. Herbinet, P.A. Glaude, A. Konnov, F. Battin- Leclerc, Measurements of Laminar Flame Velocity for Components of Natural Gas, *Energy Fuels 25 (2011) 3875-3884*

[21] I.V. Dyakov, A.A. Konnov, J. De Ruyck, K. J. Bosschaart, E. C. M. Brock, L. P. H. De Goey, Measurement of adiabatic burning velocity in methane-oxygen-nitrogen-mixtures, *Combustion Science and Technology 172 (2010) 81-96*

[22] N. Merlo, T. Boushaki, C. Chauveau, S. de Persis, L. Pillier, B. Sarh, I. Gökalp, Experimental Study of Oxygen Enrichment Effects on Turbulent Non-premixed Swirling Flames, *Energy Fuels 27 (2013) 6191-6197*

[23] M. Ditaranto, J. Hals, Combustion instabilities in sudden expansion oxy–fuel flames, *Combustion and Flame 146 (2006) 493–512*

[24] T. Boushaki, M.A. Mergheni, J.C. Sautet, B. Labegorre, Effects of inclined jets on turbulent oxy-flame characteristics in a triple jet burner, *Experimental Thermal and Fluid Science 32 (2008) 1363–1370*

[25] M. Ditaranto, T. Oppelt, Radiative heat flux characteristics of methane flames in oxy-fuel atmospheres, *Experimental Thermal and Fluid Science 35 (2011) 1343-1350*

[26] C.E. Baukal, B. Gebhart, Oxygen-enhanced natural gas flame radiation, *International Journal of Heat and Mass Transfer 40 (1997) 2539-2547*

[27] J.C. Sautet, L. Salentey, M. Di Taranto, Large-scale turbulent structures in non-premixed, oxygen enriched flames, *International Communications in Heat and Mass Transfer 28 (2001) 277–287*

[28] Z. Riahi, M. A. Mergheni, J.C. Sautet, S.B. Nasrallah, Experimental study of natural gas flame enriched by hydrogen and oxygen in a coaxial burner, *Applied Thermal Engineering 108 (2016) 287-295*

[29] Z. Riahi, H. Bounaouara, I. Hraiech, M. A. Mergheni, J.C. Sautet, S.B. Nasrallah, Combustion with mixed enrichment of oxygen and hydrogen in lean regime, *International Journal of Hydrogen Enery 42 (2017) 8870-8880*

[30] D.C. Wilcox, Turbulence modeling for CFD, *D C W Industries; 2nd edition, 1998*

[31] F.R. Menter, Two equation eddy-viscosity turbulence models for engineering applications, *AIAA Journal, 32 (1994) 1598-1605*

[32] W. Huang, W. Liu, S. Li, Z. Xia, J. Liu, Z. Wang, Influences of the turbulence model and the slot width on the transverse slot injection flow field in supersonic flows, *Acta Astronautica 73 (2012) 1-9*

[33] FLUENT 6.3. Tutorial Guide Fluent 6.3. Inc.; 2006

[34] B.F. Magnussen, B.H. Hjertager, On mathematical models of turbulent combustion with special emphasis on soot formation and combustion. *Technical report, 16th Symp. (Int.) on Combustion, Cambridge, MA, 1976*

[35] W.A. Fiveland, Discrete-ordinates solutions of the radiative transport equation for rectangular enclosures, *Journal of Heat Transfer 106 (*1984) *699-706*

[36] E.H. Chui, G.D. Raithby, Computation of radiant heat transfer on a non-orthogonal mesh using the finite-volume method, *Numerical Heat Transfer 23 (1993) 269-288*

[37] B.W. Li, H.G. Chen, J.H. Zhou, X.Y. Cao, K.F. Cen, The spherical surface symmetrical equal dividing angular quadrature scheme for discrete ordinates Method, *Journal Heat Transfer 124 (2002) 482-490*

[38] T.F. Smith, Z.F. Shen, J.N. Friedman, Evaluation of coefficients for the weighted sum of gray gases model, *Journal Heat Transfer 104 (1982) 602-608*

[39] A. Soufiani, E. Djavdan, A comparison between weighted sum of gray gases and statistical narrow-band radiation models for combustion applications, *Combustion and Flame 97 (1994) 240-250*

FIGURE

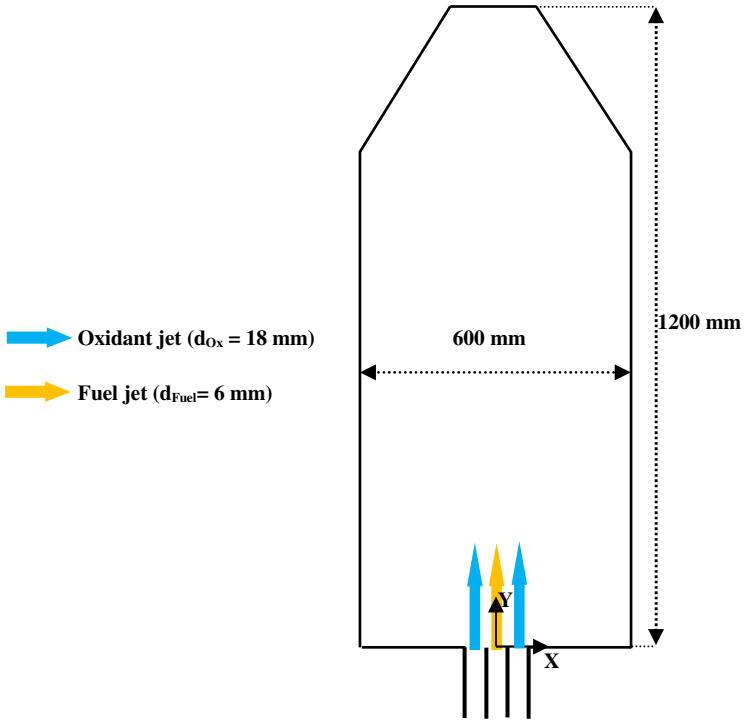

Figure.1. Schematization of the experimental configuration [22, 23]

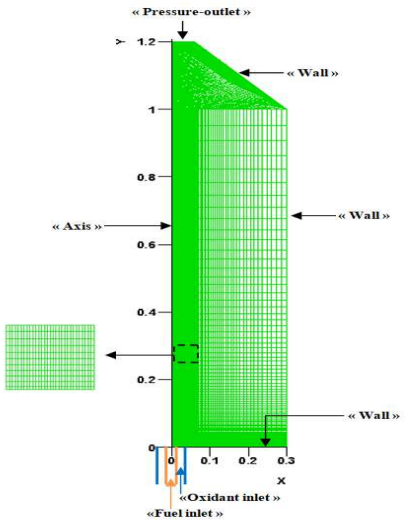

Figure.2. Calculation domain mesh and boundary conditions

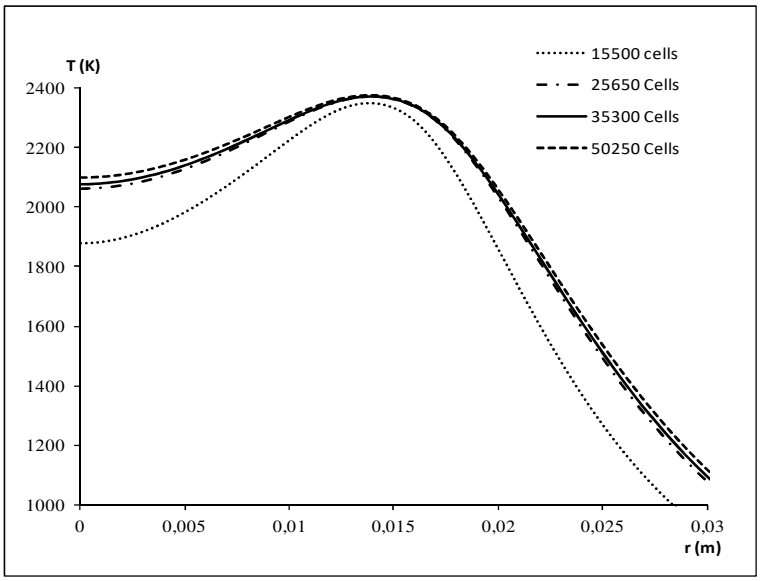

Figure.3. ***Temperature profiles for different meshes***

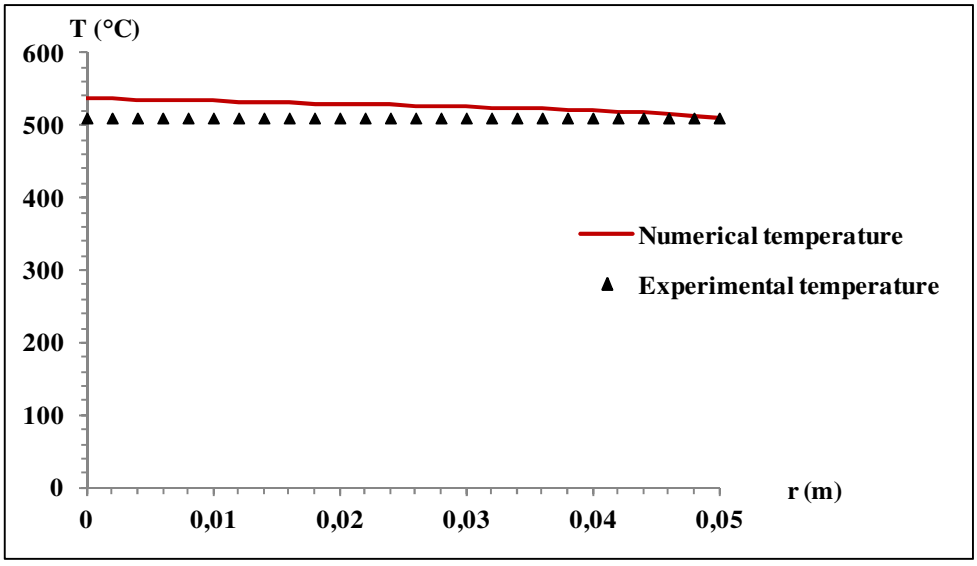

Figure.4. ***Numerical and experimental comparison of the exhaust temperature***

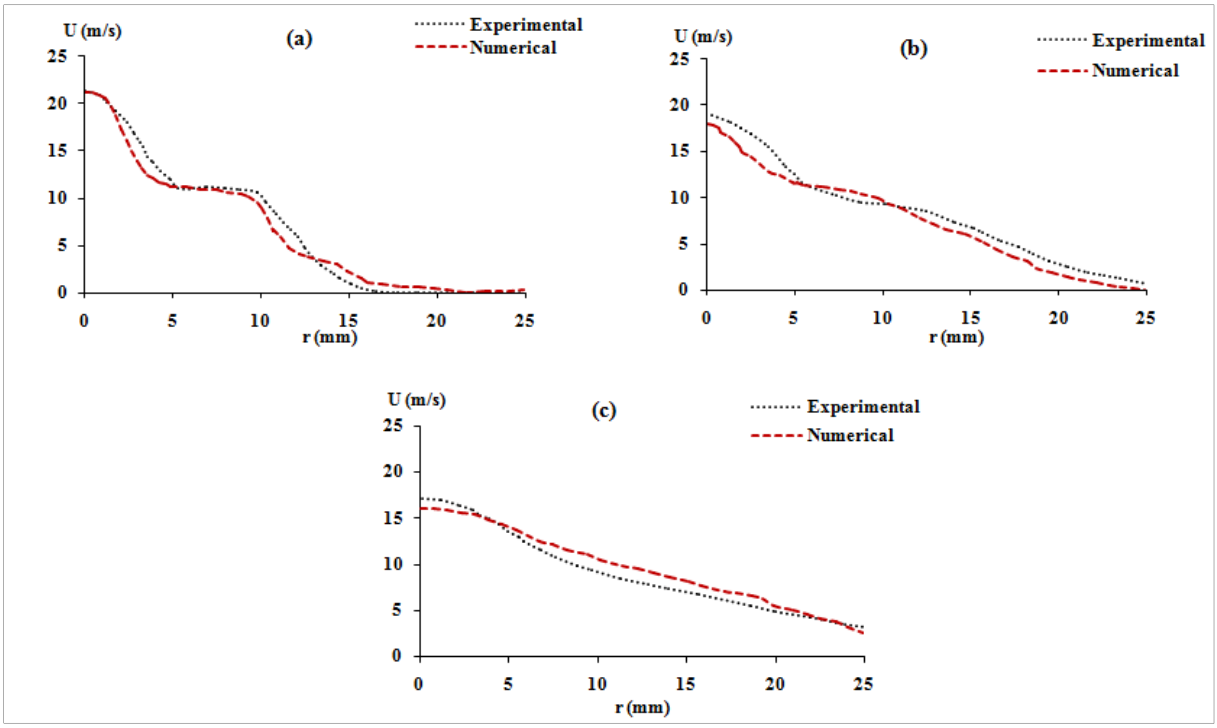

Figure.5. ***Longitudinal velocity profiles along the flame :(a) y = 20 mm; (b) y = 50 mm and (c) y = 100 mm***

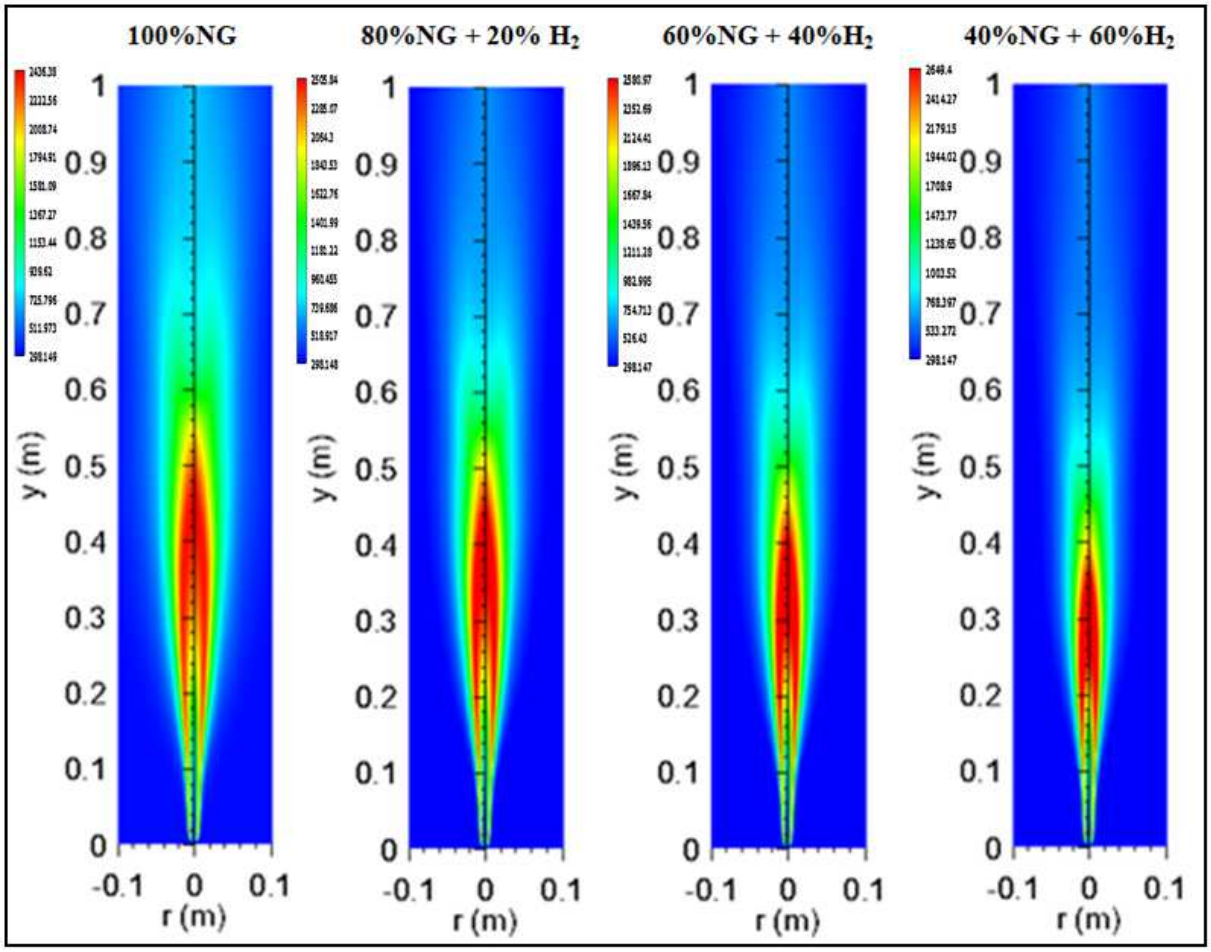

Figure.6. ***Temperature distribution***

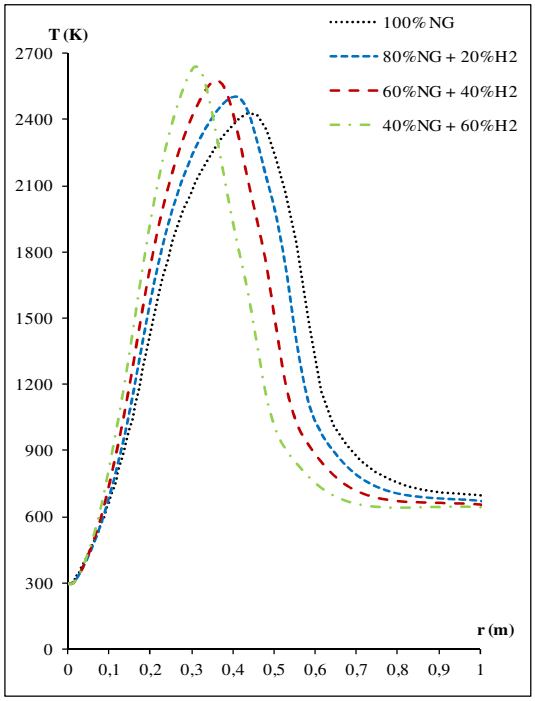

Figure.7. ***Axial temperature evolutions for different percentage of hydrogen***

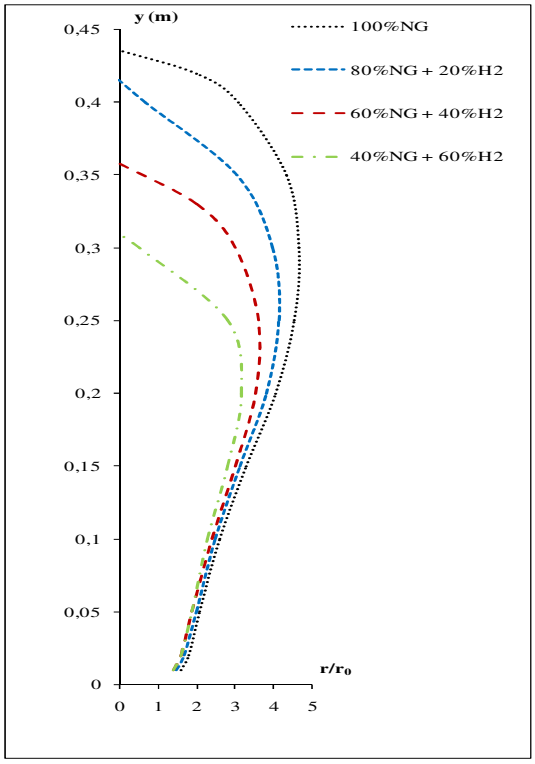

Figure.8. ***Stoichiometric lines for different hydrogen rate***

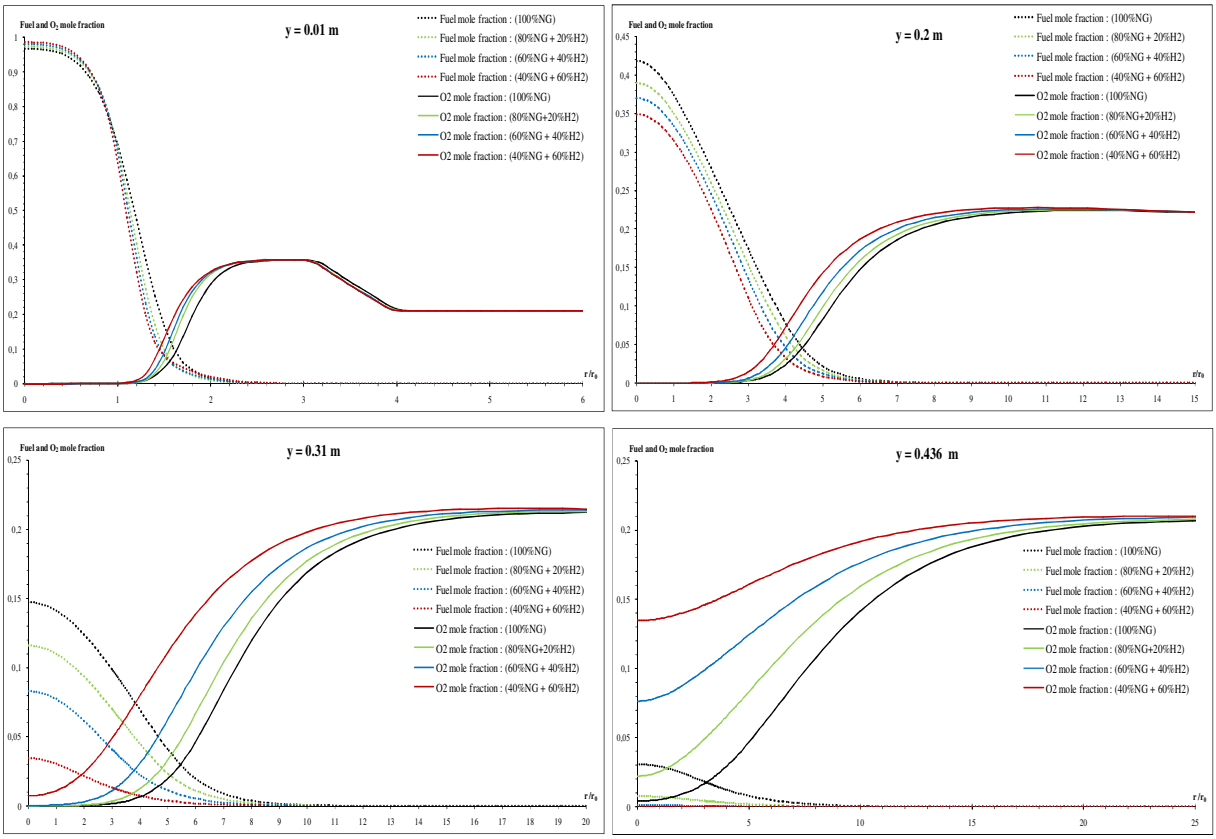

Figure.9. ***Fuel and Oxygen mole fraction***

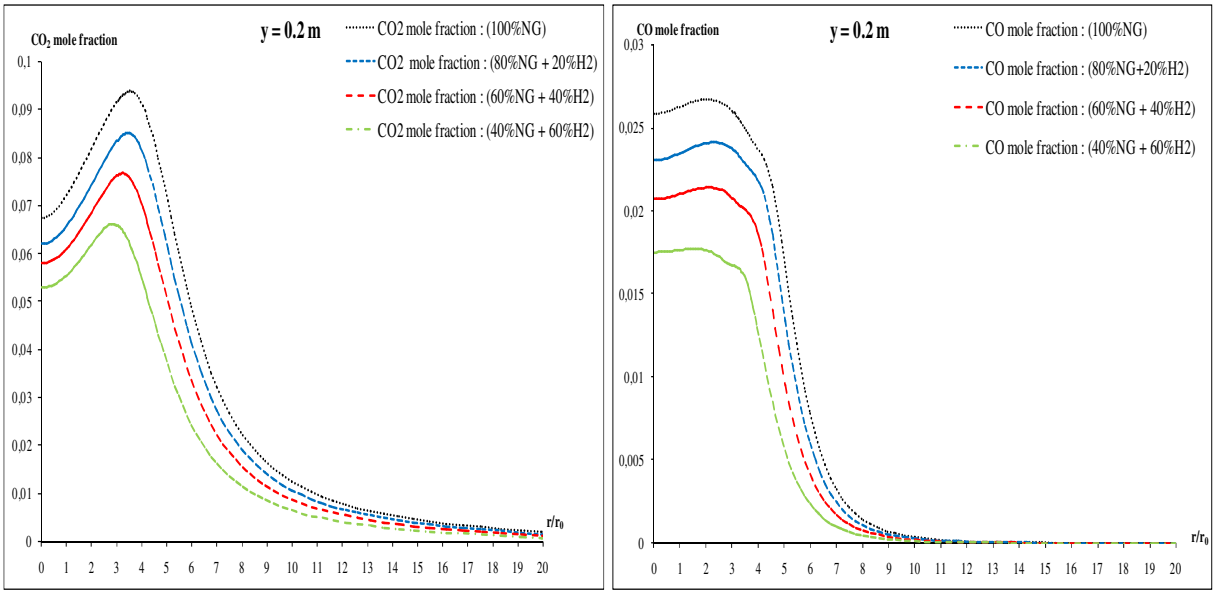

Figure.10. ***Profiles of CO_2 and CO mole fraction***

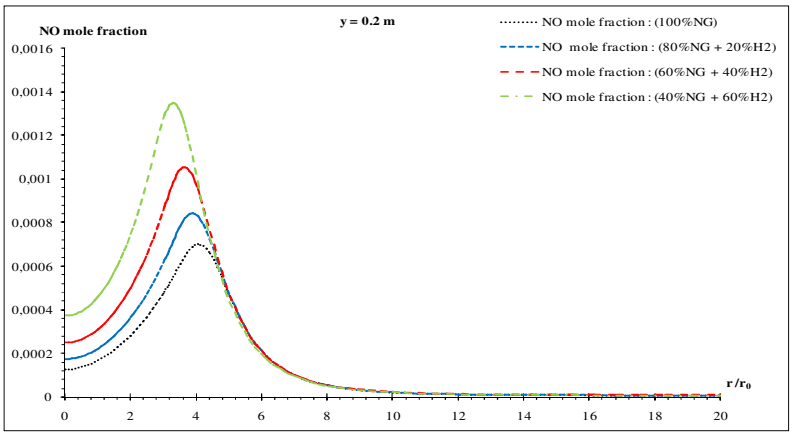

Figure.11. ***NO mole fraction***

TABLE

Table.1 ***Natural gas compositions***

Natural Gas	$X_{CH4}=0.85$
	$X_{C2H6}=0.09$
	$X_{C3H8}=0.03$
	$X_{CO2}=0.01$
	$X_{N2}=0.02$

Table.2 ***Boundary Conditions***

Domain	***Boundary conditions***	
Fuel jet	***Velocity Inlet***	d_{Fuel}= 6 mm
		X_{NG}=1;0.8;0.6 and 0.4
		X_{H2}=0;0.2;0.4 and 0.6
		V_{Fuel} = 15 m/s
		I_t = 10%
		T= 25°C
Oxidant jet	***Velocity Inlet***	d_{Ox}= 18 mm
		$X_{O2}=0.36$ } mixture 80% Air
		$X_{N2}=0.64$ } and 20% O_2
		V_{Ox} = 10 m/s
		I_t = 10%
		T= 25°C
Confinement wall	***Wall***	
Symmetry axis	***Axis***	
Exhaust gas	***Pressure-Outlet***	

Table.3 ***Flame length and maximum temperature***

	L_f (mm)	***T (K)***
100% NG	*436*	*2429*
80%NG + 20%H2	*415*	*2497*
60%NG + 40%H2	*358*	*2577*
40%NG + 60%H2	*310*	*2644*